

Journal of Materials Chemistry A

Accepted Manuscript



This is an *Accepted Manuscript*, which has been through the Royal Society of Chemistry peer review process and has been accepted for publication.

Accepted Manuscripts are published online shortly after acceptance, before technical editing, formatting and proof reading. Using this free service, authors can make their results available to the community, in citable form, before we publish the edited article. We will replace this *Accepted Manuscript* with the edited and formatted *Advance Article* as soon as it is available.

You can find more information about *Accepted Manuscripts* in the [Information for Authors](#).

Please note that technical editing may introduce minor changes to the text and/or graphics, which may alter content. The journal's standard [Terms & Conditions](#) and the [Ethical guidelines](#) still apply. In no event shall the Royal Society of Chemistry be held responsible for any errors or omissions in this *Accepted Manuscript* or any consequences arising from the use of any information it contains.

Unique Synthesis of Sandwiched Graphene@(Li_{0.893}Fe_{0.036})Co(PO₄) Nanoparticles as High-Performance Cathode Material for Lithium-Ion Battery

Li Liu^a, Huijuan Zhang^a, Xi Chen^b, Ling Fang^a, Yuanjuan Bai^a, Ruchuan Liu^b, Yu Wang^{a*}

^aThe State Key Laboratory of Mechanical Transmissions and the School of Chemistry and Chemical Engineering, Chongqing University, 174 Shazheng Street, Shapingba District, Chongqing City, P.R. China, 400044; ^bCollege of Physics, Chongqing University, No. 55 Daxuecheng South Rd., Shapingba, Chongqing, China,

E-mail: wangy@cqu.edu.cn; prospectwy@gmail.com

Supporting information for this article is available.

Keywords: (Li_{0.893}Fe_{0.036})Co(PO₄), graphene, doping, sandwiched, cathode, Lithium-ion battery

Abstract

In this report, a novel method towards synthesis of the two-layer sandwiched graphene@(Li_{0.893}Fe_{0.036})Co(PO₄) nanoparticles (SG@LFCPO) has been presented. In the approach, the sheet-like precursor, as the sacrificial template, and glucose molecules, as the carbon source, are the key factors of forming the specific morphology that both top and bottom graphene sheets tightly envelop the (Li_{0.893}Fe_{0.036})Co(PO₄) nanoparticles, just like a sandwich. Owing to the combination of various favorable conditions, such as Fe doping, coating graphene and designing morphology, the as-prepared SG@LFCPO displays very promising performances in terms of rate performance (the discharge capacity of 85 mAh g⁻¹ at 20 C), cyclability (the coulombic efficiency of around 92.6 %), stability (capacity retention of 94.6% after 100 cycles) and fast kinetics.

Introduction

In recent years, the range of application of Li-ion batteries (LIBs) has been stretched from small-sized portable electronics to large-scale electric vehicles and stationary energy storage systems. Large-scale energy applications require the batteries to be economically efficient, highly safe, highly energy and power density¹. Therefore, high-energy, low-cost and long-life electrode materials are in urgent need to maintain the momentum of LIBs². Among a variety of cathode materials, LiCoO₂ is subjected to the low structural and thermal stabilities³, leading to inadequate for next generation applications entailing higher temperatures and more aggressive conditions, although it is the most widely used cathode in extant LIBs. Recently, there has been interest in the use of lithium transition metal phosphates with olivine structure LiMPO₄ (M=Fe, Mn and Co) as potential cathode materials for LIBs^{2,4-6}. The theoretical capacity of LiMPO₄ (170 mAh g⁻¹) provides higher energy density than that of LiCoO₂^{6,7}. Besides, LiMPO₄ possesses the strong P-O covalent bonds resulting in thermodynamical and dynamical stability at high temperature and charge state⁸. Among the LiMPO₄ family, LiFePO₄ has been widely researched and commercially produced, owing to the eco-friendliness and thermal stability⁹⁻¹². LiMnPO₄ is another promising cathode material with a higher operating voltage at ~4.1 V^{13,14}. However, LiFePO₄ is limited by its low discharge potential (3.4 V vs Li/Li⁺) and LiMnPO₄ sustains Jahn-Teller distortion and large volume change during the charge-discharge cycles^{13,14}. For these reasons, LiCoPO₄ has attracted plenty of attentions even though Co is often considered an expensive element, in fact, LiCoPO₄ is expected to be cheaper than all commercialized LIBs on the market (due to the improved energy density)¹⁵. LiCoPO₄ has advantages of flat high potential (at approximately 4.8 V vs Li/Li⁺), good theoretical capacity (167 mAh g⁻¹) and smaller structure volume change^{2,16}. However, there are some drawbacks and unsolved problems for this high-voltage cathode material. The practical use of LiCoPO₄ is precluded by its poor rate cycling ability related to the inherently low electrical conductivity (< 10⁻⁹ S cm⁻¹) and

Li^+ ionic conductivity^{17, 18}. Besides, it suffers from capacity fade caused by structure deterioration and electrolyte decomposition¹⁹⁻²¹.

Consequently, many studies have focused on facilitating Li ionization and improving electrical conductivity, e.g., doping metal ions, coating electrically conductive materials and shortening Li^+ diffusion paths²²⁻²⁵. While Cu, Cr, Mn, Al, Zr and Ni doping improve the electrochemical performance of LiCoPO_4 ,^{22, 26-31} doping-induced atomic-scale changes in structure and composition of LiCoPO_4 that lead to enhanced properties are yet to be revealed and fully exploited³². As we all know, Fe, as environment friendly and low-price material, possesses an advantage of excellent electronic conductivity, thus doping LiCoPO_4 with Fe has been pursued to enhance electronic conduction and make cost down. Meanwhile, coating LiCoPO_4 particles with conductive materials can improve electronic conductivity and protect particles from agglomeration at high synthesis temperature, desirable for facile lithium transport and better electrochemical properties³³. From another point of view, down-sizing LiCoPO_4 has been shown to improve the electrochemical performance due to the shortening of Li^+ diffusion distance^{13, 34}.

In consideration of those reasons, a sandwich-like graphene-based composite, in which monodispersed nanoparticles are encapsulated in sandwiched graphene sheets, has been successfully fabricated. According to prof. wang, et al.³⁵, the unique morphology has a synergic effect on the electrochemical performance for LIBs application. In the synthetic process, a hydrated sheet-like precursor has been prepared and submerged in 1M FeCl_2 for 10 h. Then making use of the hydrogen-bond interaction, glucose molecules combine with the hydroxyls on the surface of sheet-like precursors to form the polymer-layers, which are graphitized into graphene sheets in sequence by calcinations in the argon atmosphere. In the meantime, the samples decompose and release CO_2 , NH_3 , H_2O gas, forming the pore in the sandwiched structure. Following that, the precursors recrystallize into $(\text{Li}_{0.893}\text{Fe}_{0.036})\text{Co}(\text{PO}_4)$ nanoparticles. In the structure, the sandwiched graphene sheets tightly envelop the $(\text{Li}_{0.893}\text{Fe}_{0.036})\text{Co}(\text{PO}_4)$ nanoparticles to suppress the direct contact between electrolyte and active nanoparticles, decreasing the capacity loss. Obviously, Fe and graphene are favourable conductors, therefore the introduction of Fe and the formation of graphene could improve the electronic conductivity, speeding up the reaction kinetics. Furthermore, the pore in the novel structure might buffer the local volume change during the lithium insertion/extraction cycling, improving the structural stability of the electrode material. More importantly, the novel morphology with contractible active nanoparticles offers a shorter Li^+ diffusion pathway, enhancing the rate performance. To the best of our knowledge, these results first provide insights that pave the way for the rational design of the two-layer sandwiched graphene@ $(\text{Li}_{0.893}\text{Fe}_{0.036})\text{Co}(\text{PO}_4)$ nanoparticles as the cathode materials for LIBs and related applications.

Results and discussion

The fabrication process of the SG@LFCPO is schematically depicted in Scheme. 1. The sheet-like precursors were first synthesized and submerged in 1M FeCl_2 at room temperature for 10 h. Then the glucose molecules combined with the hydroxyls on the surface of the precursors by means of hydrogen-bonding interaction to form uniformly polymerized membranes, during the hydrothermal reaction. Following that, the solid-state reaction between the above obtained intermediate product and LiH_2PO_4 at the molar ratio of 1.1:1 was carried out at 720 °C in Ar atmosphere. At the moment, the polymerized films would be graphitized into graphene sheets and the decomposable groups of the precursors would be decomposed to generate a mass of vacancies. Meanwhile, the precursors would shrink and aggregate, separately circling the individual crystallization centers to be recrystallized into nanoparticles, encapsulated by both top and bottom graphene sheets, on multiple sites.

The as-obtained SG@LFCPO and pristine LiCoPO_4 nanomesh were initially characterized by X-ray diffraction (XRD) to identify the crystallographic structure and crystallinity, shown in Figure 1. The patterns can be assigned to well-crystallized orthorhombic olivine structure of $(\text{Li}_{0.893}\text{Fe}_{0.036})\text{Co}(\text{PO}_4)$ (JCPDS No. 89-6193) and LiCoPO_4

(JCPDS No. 89-6192), respectively. No other peaks were observed for impurities. In XRD pattern for the SG@LFCPO, the peak at 2θ of 31° (Co K_α) which represents to the existence of graphene. Besides, the XRD pattern (Figure S1 support information) reveals that the sheet-like precursor is highly crystalline. The crystal parameters of Fe-doped LiCoPO₄ and non-doped LiCoPO₄, calculated by jade 5.0 software, are listed in Table 1. We find that for (Li_{0.893}Fe_{0.036})Co(PO₄), the lattice parameter *b* is smaller than that of pure LiCoPO₄ while lattice parameters *a* and *c* slightly increase. For the reason that Li⁺ diffusion energy is orientation-dependent which is the lowest for the pathway along the [010] channel, that is to say, along *b* axis direction in olivine structure^{36, 37}, as atomic model shown in Figure 2, the lattice parameters *a* and *c* little increase, suggesting the Fe-doped LiCoPO₄ has a slightly wider Li⁺ diffuse pathway. And that, the lattice parameter *b* becomes smaller, demonstrating a shorter Li⁺ diffuse pathway. All of them reveal that Fe doping is benefit to fast Li⁺ diffusing, which was also certified in the paper related to Na-doped LiCoPO₄³⁸. Besides, we have got the Raman spectroscopy of SG@LFCPO, exhibited in Figure S2. The Raman bands at 1581.2 (G band) arising from the first order scattering of the E_{2g} phonon of sp² C atoms, and 1328.3 cm⁻¹ (D band) arising from a breathing mode of *k*-point photons of A_{1g} symmetry, are observed for SG@LFCPO, confirming the existence of graphene in the composite.

The morphology and thickness of as-obtained products were examined using scanning electron microscope (SEM) and atomic force microscope (AFM), respectively. Combined with the SEM image (shown in Figure 3a), the AFM image (Figure S3a) and the XRD pattern (Figure S1), we can see that the precursors possess a number of characteristics, such as high crystallinity (testified by the XRD pattern), 2-dimensional, ultra-thin down to ~10 nm (verified by the AFM image), uniformed shape and large dimensions from several hundreds of square nanometers to tens of square micrometers (observed in the SEM image). As seen in Figure 3b, the large scale samples have been obtained, illustrating the method would be applied in large-scale commercial production. The SEM in Fig 3c displays that LFCPO nanoparticles homogeneously disperse in the double-layer sandwiched graphene sheets and separate from each other. What's more, according to the Figure 3c, the diameters of these LFCPO nanoparticles fall into a range of 40-80 nm. From the inset image in the Figure 3c, we know that the thickness of SG@LFCPO is estimated about 5-10 nm, in well agreement with the AFM image. Figure S4a shows the SEM image of pristine LiCoPO₄ nanomeshes, which is used to the contrast experiment. On account of the decomposition of the labile units, such as ammonium, hydrate and hydroxyl groups, a number of vacancies are formed for the pristine LiCoPO₄ nanomeshes. Figure 3d displays the EDS spectra of the SG@LFCPO, which demonstrates the composites contain C, Fe, Co, P and Si elements, wherein Si comes from the silicon substrates. Moreover, the Fe/Co ratio achieved from the EDS spectroscopy (Figure 3d) is close to 1: 0.04, in accordance with the XRD and XPS results. To further clarify the exact composition of the materials, the ICP-AES is conducted to obtain the elemental ratio of Li/Fe/Co, as shown in Table 2. As is expected, the result from Table 2 conforms to that of EDS and XPS, illustrating effectively the as-prepared material is (Li_{0.893}Fe_{0.036})Co(PO₄) phase with the exact composition. What's more the carbon content in the composite is about 7.6 wt% (see the Experimental Section).

The transmission electron microscopy (TEM) is a powerful characterization tool to provide more insight into the composition and microstructure of the materials. The especial morphology of the as-prepared SG@LFCPO is exhibited in Figure 4a. Obviously, the LFCPO nanoparticles are monodispersed through the two-dimensional structure and do not stack to form an agglomerated structure on the supported graphene sheets, implying the existence of double-layer graphene can prevents the nanoparticles from aggregating. According to magnified TEM image, shown in Figure 4b, the grain sizes of LFCPO nanoparticles have no difference with that in Figure 3c. The TEM image, in the Figure S4b, indicates that sheet-like precursor with regular morphology is ultrathin, which would be inherited from precursors to produces. Figure S4c shows the TEM image of pristine LiCoPO₄ nanomesh with porous sheet-like structure. High-resolution transmission electron microscope (HRTEM) image of SG@LFCPO, shown in Figure 4c, verifies an individual LFCPO nanoparticle with well-crystallized nature, as the white

circles indicated. The graphene is obviously observed outside the white circle, demonstrating the graphene tightly parcel the active nanoparticles. Furthermore, along two mutually-perpendicular directions, there are fringes whose spacings are calculated to be 0.24 and 0.51 nm, corresponding to (002) and (200) crystal planes in orthorhombic $(\text{Li}_{0.893}\text{Fe}_{0.036})\text{Co}(\text{PO}_4)$, respectively. The results show that the thinnest part of the SG@LFCPO is along the *b*-axis, which is favorable direction for the Li^+ diffusion. According to the AFM image, in Figure S3b, the thickness of SG@LFCPO is estimated to be ~ 10 nm, which reveals a short Li^+ diffusion pathway and a fast Li^+ diffusion kinetics. The Brunauer-Emmett-Teller (BET) measurement was performed to determine the surface area and pore size distribution of SG@LFCPO and pristine LiCoPO_4 nanomesh, respectively. Figure 4d reveals that the surface area of SG@LFCPO is up to $280.6 \text{ m}^2\text{g}^{-1}$, meanwhile, the pore size is centered at around 4.85 nm (inset of Figure 4d). However, the specific surface area of $52.57 \text{ m}^2\text{g}^{-1}$ is achieved for pristine LiCoPO_4 nanomesh, according to Figure S4d, and the pore size is mainly distributed around 6.12 nm. Therefore, it can be seen that designing novel morphology could increase the specific surface area and voidage, facilitating the transmission of electrolyte. The elemental mappings of the SG@LFCPO based on Figure S5a are displayed in Figure S5b-5f, from which it can be observed that C, O, Co, Fe and P elements are homogeneously distributed. The above results suggest that the SG@LFCPO would exhibit a good electrochemical performance for electrolyte flooding and Li^+ diffusion.

In order to confirm the valence states of the elements present in the $(\text{Li}_{0.893}\text{Fe}_{0.036})\text{Co}(\text{PO}_4)$ composite, X-ray photoelectron spectroscopy (XPS) measurement was carried out, and the corresponding spectra displayed in Figure S6 after calibrating by the standard XPS peak of C1s. The observed C1s peak at 284.8 eV mainly represents graphitic carbon³⁹. The peak binding energy at 532.8 eV, in Figure S6b, is attributed to O1s of P-O-P bond⁴⁰. Besides, the P2p band is observed at 133.8 eV for P2p_{3/2}, which is consistent with the value reported for P⁵⁺ in PO₄⁴¹. The Figure S6d and S6e clearly show the presence of Fe2p and Co3p core levels with no trace of impurities. The core level photoelectron peaks at 710.8 eV is well assigned to Fe2p_{3/2}, suggesting Fe is in divalent state in agreement with previous works⁴². In addition, the Co3p level is observed at 60.8 eV for Co3p_{3/2}, which may be due to spin orbital interactions, indicating the presence of Co²⁺⁴³.

The electrochemical performances of SG@LFCPO are investigated using Li metal as anode at various current densities between 2.5 and 4.95 V vs. Li/Li^+ . The typical charge-discharge curves of the SG@LFCPO for different cycles at 0.1 C rate are displayed in Figure 5a. The discharge curves only showing one plateau can be supported by the one-step mechanism of lithium deintercalation⁴⁴. All the discharge curves exhibit a wide and flat voltage plateau at approximately 4.72 V, implying the electrode structure is stable in the voltage range. In the initial charging/discharging cycle, the reaction between the active material of electrode and electrolyte leads to the decomposition of the electrolyte and the formation of SEI film on the electrode, causing that the initial discharge capacity is much less than charge capacity. From the second cycle, however, the discharge capacity lose is gradually diminished. The discharge capacities are approximately 150, 148, 147 and 142 mAh g⁻¹ at the 2nd, 10th, 50th and 100th cycles, respectively, demonstrating the outstanding capacity retention of 94.6% for SG@LFCPO. However, when it comes to the charge-discharge curves of pristine LiCoPO_4 nanomesh in Figure 5b, we can see a fast recession of discharge capacity in the wake of incremental cycle-index. The contrast of Figure 5a and 5b indicates that coating graphene and Fe doping are in favour of the structure stability. Of course, the cyclic voltammetry (CV) measurement is adopted to investigate the electrochemical characteristics, as shown in Figure S7a. The oxidation peak and reduction peak at ~ 4.72 and ~ 4.66 V, respectively, are attributed to the redox reaction of $\text{Co}^{2+}/\text{Co}^{3+}$, in accordance with the results of charge-discharge curves. Besides, it can be seen that except for the first cycle, the curves in the subsequent cycles follow almost same path, indicating high stability and reversibility for Li^+ insertion and extraction. And the potential difference between the two peaks is less than 0.1 V, suggesting an excellent rate performance. Because of the importance in evaluating total performance, the rate performances of SG@LFCPO and pristine LiCoPO_4 nanomesh were researched in Figure 5c. The cells were first cycled at 0.1 C for

10 cycles, followed by cycling with a stepwise increase of the discharge current densities to as high as 20 C. A highly average discharge capacity of 85 mAh g⁻¹ was obtained at the highest current density of 20 C, conversely, the rest of discharge capacity is a little for pristine LiCoPO₄ nanomesh. Moreover, at the rates of 0.1, 1, 5 and 10 C, the corresponding discharge capacities were 150, 145, 129 and 104 mAh g⁻¹ for SG@LFCPO, versus 118, 93, 67 and 35 mAh g⁻¹ for pristine LiCoPO₄ nanomesh. When the discharge rate was changed back to 0.1 C after the high-rate charge-discharge cycling, the reversible discharge capacity of SG@LFCPO returned to 148 mAh g⁻¹. Obviously, the SG@LFCPO reveals much better rate performance than the pristine LiCoPO₄ counterpart. The galvanostatic measurement at a rate of 0.1 C is shown in Figure 5d to present the coulombic efficiency, cyclability and specific capacity upon 100 cycles. It's easy to discover that the charge and discharge capacities slightly descend after 100 cycles. Except the initial cycle, the charge capacity and discharge capacity of SG@LFCPO can be retained at ~162 and 150 mAh g⁻¹, respectively, with a high coulombic efficiency of around 92.6 %. Interestingly, the coulombic efficiencies of the first several cycles are relatively lower than those of the subsequent cycles. The possible reason is that the active materials couldn't completely contact with electrolyte in the first several cycles, causing the capacity's decrease. As redox reaction proceeds, the electrolyte penetrates into the inner part of the void space, resulting in the increased capacities. However, as shown in Figure S7b, the discharge capacity of pristine LiCoPO₄ nanomesh declines 52 mAh g⁻¹ and the capacity retention is 56.7 % after 100 cycles, which are tremendously inferior to those of SG@LFCPO. Figure S8 shows the SEM image of SG@LFCPO after electrochemical testing. As shown in Figure S8, although the aggregation of the SG@LFCPO after electrochemical testing is observed, the structure of two-layer sandwiched graphene@(Li_{0.893}Fe_{0.036})Co(PO₄) nanoparticles has been reserved, further supporting the claims of the excellent stability and cyclability. Owing to the fact that operating temperature is also a determiner of cell performance, herein, the temperature-dependent Li storage and rate performance of the SG@LFCPO have been studied, shown in Figure S7c and S7d. At the testing temperature of 50 °C, the delivered capacity at a rate of 0.1 C is the highest, while the cycling stability is the worst. The reason is that the activation of electrode materials could be accelerated by the high temperature, in favour of the discharge capacity. On the contrary, the high temperature could accelerate the severe decompositions of the electrolyte to release some gas, such as HF, PF₅, etc, leading to the increscent internal pressure and deformation of battery. Thus the cyclability at 50 °C is inferior to 25 and 0 °C, however, the rate performance is gradually increased with the testing temperature varying from 0, 25 and 50 °C. The electrochemical impedance spectroscopy (EIS) data of SG@LFCPO and LiCoPO₄ nanomesh are shown in Figure S9. The impedance spectra for both samples show a single semi-circle at higher frequency followed by a straight line at a slope of approximately 45° at lower frequency. The semi-circle at higher frequency is assigned to the charge transfer resistance (R_{ct}), related to electrochemical reaction. It can be seen that formation of graphene encapsulating outside and the introduction of Fe into LiCoPO₄ could remarkably reduce the value of R_{ct}, indicating an enhancement in the kinetics and the consequent improvement in high-rate capabilities.

Those results herein give clear evidences that compared with pristine LiCoPO₄ nanomesh, SG@LFCPO possesses preferable electrochemical performances, for instance superior rate performance, outstanding cyclability, admirable stability and fast kinetics of extraction/insertion Li⁺. The improvements arise from three major factors, which are Fe doping, coating graphene and designing the novel morphology. In the first place, Fe, as an excellent conductive material, could compensate the poor electronic conductivity for LiCoPO₄. Besides, the lattice parameter *a* lightly increases and *b* tinily diminishes after Fe doping, resulting in a shorter and wider Li⁺ diffusion pathway. As we all know, the operating voltage of LiCoPO₄ is very high, however, electrolyte is easy to decompose at high voltage. This problem can be solved by coating graphene to reduce the direct contact between electrolyte and active material, enhancing the capacity retention. On the other hand, designing the porous morphology that sandwiched graphene sheets tightly envelop functional nanoparticles could shorten the Li⁺

diffusion channel. In addition, the existence of void space could buffer the volume changes during the insertion/extraction of Li^+ , improving the cyclability of cathode material.

Conclusion

In this work, the two-layer sandwiched graphene@ $(\text{Li}_{0.893}\text{Fe}_{0.036})\text{Co}(\text{PO}_4)$ nanoparticles have been successfully fabricated through the template-sacrificial method. The sheet-like precursors, as the template, and glucose molecules, as the carbon source, are the key factors of the synthetic process, contributing to the novel morphology that the LFCPO nanoparticles were tightly enveloped by the sandwiched graphene sheets. The as-prepared SG@LFCPO, with an ultrathin thickness of approximately 10 nm and the surface area of $280.6 \text{ m}^2 \text{ g}^{-1}$, display very promising performances in terms of rate performance (the discharge capacity of 85 mAh g^{-1} at 20 C), cyclability (the coulombic efficiency of around 92.6 %), stability (capacity retention of 94.6% after 100 cycles) and fast kinetics due to the combination of various favorable conditions. Undoubtedly, our research provides key insights that pave the way for the rational design and realization of graphene-based materials for LIBs and related applications.

Experimental Section

Materials: All chemicals or materials were utilized directly without any further purification before use: ethylene glycol (Fisher Chemical, 99.99 %), ammonium hydroxide ($\text{NH}_3 \cdot \text{H}_2\text{O}$, 28–30 wt %, J. T. Baker), cobalt nitrate ($\text{Co}(\text{NO}_3)_2 \cdot 6\text{H}_2\text{O}$, 99.9 %, Aldrich), sodium carbonate (Na_2CO_3 , 99.9 %, Aldrich), ferrous chloride (FeCl_2 , 99.9 %, Aldrich), Lithium dihydrogen phosphate (LiH_2PO_4 , 99.9 %, Aldrich) and anhydrous ethanol (Fisher Chemical, 99.99 %).

Preparation of $(\text{NH}_4)_2\text{Co}_8(\text{CO}_3)_6(\text{OH})_6 \cdot 4\text{H}_2\text{O}$ nanosheets: $(\text{NH}_4)_2\text{Co}_8(\text{CO}_3)_6(\text{OH})_6 \cdot 4\text{H}_2\text{O}$ nanosheets were synthesized by a hydrothermal reaction. Ethylene glycol (12.5 mL), concentrated $\text{NH}_3 \cdot \text{H}_2\text{O}$ (12.5 mL), 1M Na_2CO_3 aqueous solution (5 mL), and 1M $\text{Co}(\text{NO}_3)_2$ aqueous solution (5 mL) were mixed step-by-step under strong stirring with intervals of 1-2 min. After that, the precursor solution was stirred for another 20 mins. Then, the mixture changed into a deep pink-violet homogeneous solution. Once the mixture solution was transferred into a Teflon-lined stainless steel autoclave with a volume of 45 mL, a thermal treatment was performed for the Teflon-liner in an electric oven at 170 °C for 17 h. After the autoclave was cooled down naturally to room temperature in air, samples deposited at the bottom were collected and washed by centrifugation for at least three cycles using deionized water (D.I. water) and two cycles using anhydrous ethanol. Finally, the as-synthesized samples were then dried in a vacuum oven at 60 °C overnight to remove the absorbed water for the subsequent fabrications and characterizations.

Preparation of SG@LFCPO and the LiCoPO_4 nanomesh: $(\text{NH}_4)_2\text{Co}_8(\text{CO}_3)_6(\text{OH})_6 \cdot 4\text{H}_2\text{O}$ nanosheets (100 mg) were immersed in 1M FeCl_2 aqueous solution for 10h. Then, the samples were centrifuged for the same steps. Following that, the as-synthesized samples were dried in a vacuum oven at 60 °C overnight. The Fe-doped $(\text{NH}_4)_2\text{Co}_8(\text{CO}_3)_6(\text{OH})_6 \cdot 4\text{H}_2\text{O}$ nanosheets (100 mg) were ultrasonically mixed with glucose aqueous solution (5 mL 1M) together with additional deionized water (25 mL) to form homogeneous solution. The above mixed solution was poured into a 45 mL Teflon-lined stainless steel autoclave and sealed tightly. Next, the liner was heated in electric oven at 180 °C for 8 h. After that, the sample was washed using centrifugation for the same method, and then dried at 60 °C overnight. Then, the above samples were converted to the SG@LFCPO when the samples (130.18 mg) reacted with LiH_2PO_4 (114.32 mg) at 720 °C under Ar atmosphere in the tube furnace. For the synthesis of LiCoPO_4 nanomesh, the experimental procedures followed the same processes as the SG@LFCPO except immersion in FeCl_2 solution and hydrothermal reaction with glucose aqueous solution.

Characterization of the samples: field-emission SEM (JEOL JSM-7800F) coupled with an EDS analyzer (JEOL, JSM-7800F), TEM coupled with an EDX analyzer (Philips, Tecnai, F30, 300 kV), X-ray photoelectron spectrometry with a ESCALAB250 analyzer (XPS), powder X-ray diffraction (Bruker D8 Advance X-ray diffractometer with Co K_α radiation ($\lambda = 1.78897 \text{ \AA}$)), Brunauer-Emmett-Teller surface area measurement (BET, Quantachrome Autosorb-6B surface area and Pore size analyzer), Raman spectroscopy (RENISHAW Invia Raman Microscope, voltage (AC) 100-240 V, power 150 W), Atomic Force Microscope (AFM, Asylum Research, MFP-3D) were used to characterize the obtained samples. The elementary compositions of the materials were determined by inductive coupled plasma-atomic emission spectroscopy (ICP-AES, iCAP 6300 Duo).

Carbon content tests: Firstly, 200.00 mg of the samples (SG@LFCPO) were added in concentrated hydrochloric acid. After 24 hours' stirring, the $(\text{Li}_{0.893}\text{Fe}_{0.036})\text{Co}(\text{PO}_4)$ nanoparticles were completely dissolved in acid. Then the undissolving carbon was collected and washed with deionized water and anhydrous ethanol. Following that, the carbon was dried in an oven at 60 °C overnight to remove absorbed water and ethanol. The carbon weight measurements were taken using a Merrler-Toledo analytical balance. The carbon content of SG@LFCPO was then calculated using the formula:

$$C\% = W(\text{C}) / W(\text{SG@LFCPO}) \times 100\%$$

Where $W(C)$ and $W(SG@LFCPO)$ were the weight of carbon and $SG@LFCPO$, respectively. The results show that the carbon content in the as-prepared material is approximately 7.6 wt% by calculation. For comparison, the $(Li_{0.893}Fe_{0.036})Co(PO_4)$ particles (200 mg) without coating carbon were synthesized and dissolved in concentrated hydrochloric acid with the same process.

Electrochemical testing: A homogeneous mixture composed of the $SG@LFCPO$, carbon black, and polyvinyl difluoride (PVDF) using 1-methyl-2-pyrrolidinone (NMP) as solvent in a weight ratio of 80:15:5 was prepared under strong magnetic stirring for at least 1 d. Then some of the mixture was extracted and spread onto Al foils. Before and after the samples were spread, the Al foils were weighed using a high-precision analytical balance. The read difference was the exact mass for the coated samples on Al foils. Normally, the sample loadings range from 1.2 to 1.6 $mg \cdot cm^{-2}$. The obtained pieces of Al covered with samples were then used as working electrodes with 1M $LiPF_6$ in ethylene carbonate and diethyl carbonate (EC/DMC=1:1 v/v) as electrolyte. Celgard 2400 was applied as the separator film to isolate the two electrodes. Pure Li foil (99.9%, Aldrich) served as the counter electrode and reference electrode. The cell was assembled in an argon filled glove box in which moisture and oxygen concentrations were strictly limited to below 0.1 ppm. The galvanostatic cycling was performed using a Neware battery testing system (model 5V 5mA), and CV data was recorded at a scanning rate of 0.1 $mV s^{-1}$ between 2.5 and 4.95 V using an Autolab (model AUT71740) in a three-electrode cell. For the Electrochemical impedance spectroscopy (EIS) measurements, the open circuit potential (OCP) was determined first and then the AC potential was set at ± 10 mV (rms) around the OCP. A frequency range of 0.01 Hz to 100 Hz was performed by the CHI604E Electrochemical Analyzer to ensure data quality for subsequent model fitting. Then, the data acquired from the impedance testing were analyzed using Zview Version 3.2c-software.

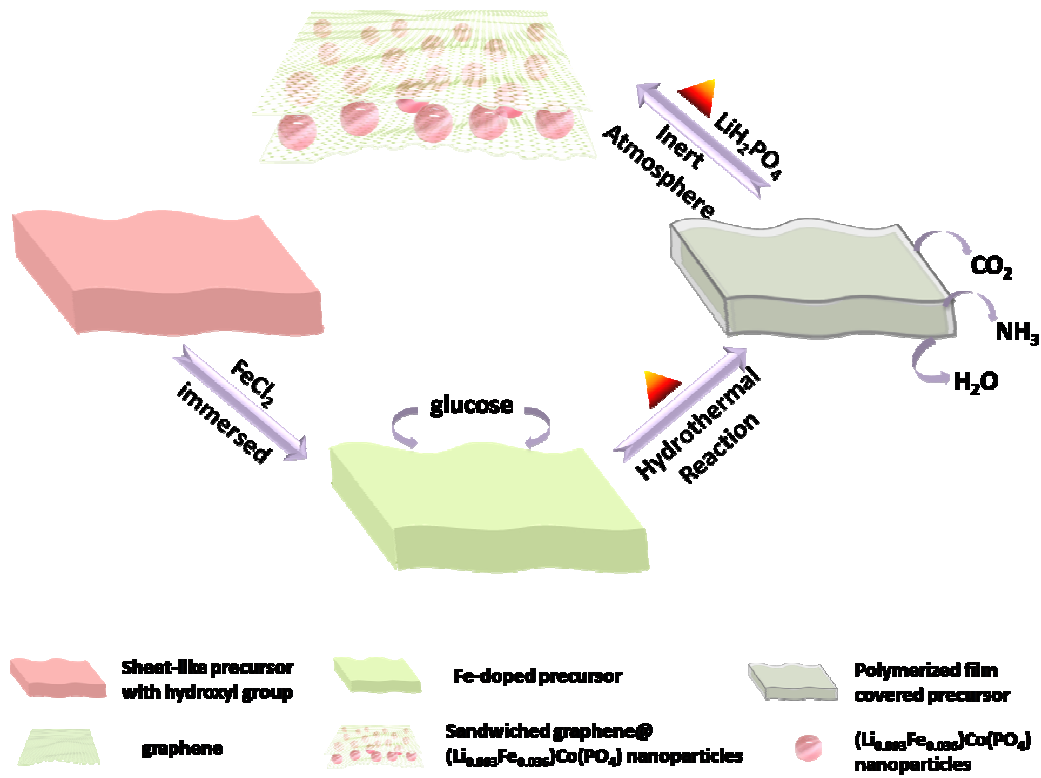
Acknowledgements

This work was financially supported by the Thousand Young Talents Program of the Chinese Central Government (Grant No.0220002102003), National Natural Science Foundation of China (NSFC, Grant No. 21373280, 21403019), Beijing National Laboratory for Molecular Sciences (BNLMS) and Hundred Talents Program at Chongqing University (Grant No. 0903005203205).

References and Notes:

1. N. R. Khasanova, O. A. Drozhzhin, S. S. Fedotov, D. A. Storozhilova, R. V. Panin and E. V. Antipov, *Beilstein J. Nanotechnol.*, 2013, **4**, 860-867.
2. K. Amine, H. Yasuda and M. Yamachi, *Electrochem. Solid-State Lett.*, 2000, **3**, 178-179.
3. M. S. Whittingham, *Chem. Rev.*, 2004, **104**, 4271-4301.
4. A. K. Padhi, K. S. Nanjundaswamy and J. B. Goodenough, *J. Electrochem. Soc.*, 1997, **144**, 1188-1194.
5. J. Carrasco, N. Lopez and F. Illas, *Phys. Rev. Lett.*, 2004, **93**.
6. A. Yamada and S.-C. Chung, *J. Electrochem. Soc.*, 2001, **148**, A960-A967.
7. K.-F. Hsu, S.-Y. Tsay and B.-J. Hwang, *J. Mater. Chem.*, 2004, **14**, 2690-2695.
8. Q. D. Truong, M. K. Devaraju, Y. Ganbe, T. Tomai and I. Honma, *Sci. Rep.*, 2014, **4**.
9. C. Delmas, M. Maccario, L. Croguennec, F. Le Cras and F. Weill, *Nat. Mater.*, 2008, **7**, 665-671.
10. S. W. Oh, S.-T. Myung, S.-M. Oh, K. H. Oh, K. Amine, B. Scrosati and Y.-K. Sun, *Adv. Mater.*, 2010, **22**, 4842-4845.
11. W.-J. Zhang, *J. Electrochem. Soc.*, 2010, **157**, A1040-A1046.
12. B. Kang and G. Ceder, *Nature*, 2009, **458**, 190-193.
13. T. N. L. Doan and I. Taniguchi, *J. Power Sources*, 2011, **196**, 1399-1408.
14. D. Rangappa, K. Sone, Y. Zhou, T. Kudo and I. Honma, *J. Mater. Chem.*, 2011, **21**, 15813-15818.
15. J. L. Allen, J. L. Allen, S. A. Delp and T. R. Jow, *ECS Trans.*, 2014, **61**, 63-68.
16. S. Okada, S. Sawa, Y. Uebou, M. Egashira, J. Yamaki, M. Tabuchi, H. Kobayashi, K. Fukumi and H. Kageyama, *Electrochemistry*, 2003, **71**, 1136-1138.
17. A. Yamada, H. Koizumi, S. I. Nishimura, N. Sonoyama, R. Kanno, M. Yonemura, T. Nakamura and Y. Kobayashi, *Nat. Mater.*, 2006, **5**, 357-360.
18. J. Wolfenstine, B. Poese and J. L. Allen, *J. Power Sources*, 2004, **138**, 281-282.
19. K. Tadanaga, F. Mizuno, A. Hayashi, T. Minami and M. Tatsumisago, *Electrochemistry*, 2003, **71**, 1192-1195.
20. N. N. Bramnik, K. G. Bramnik, C. Baetz and H. Ehrenberg, *J. Power Sources*, 2005, **145**, 74-81.
21. J. Wolfenstine, U. Lee, B. Poese and J. L. Allen, *J. Power Sources*, 2005, **144**, 226-230.
22. M. V. V. M. S. Kishore and U. V. Varadaraju, *Mater. Res. Bull.*, 2005, **40**, 1705-1712.
23. J. Wolfenstine, J. Read and J. L. Allen, *J. Power Sources*, 2007, **163**, 1070-1073.
24. Y. Hu, M. M. Doeff, R. Kostecki and R. Fiñones, *J. Electrochem. Soc.*, 2004, **151**, A1279-A1285.
25. D. Wang, H. Li, S. Shi, X. Huang and L. Chen, *Electrochim. Acta*, 2005, **50**, 2955-2958.
26. J. Wolfenstine, *J. Power Sources*, 2006, **158**, 1431-1435.
27. S.-Y. Chung, J. T. Bloking and Y.-M. Chiang, *Nat. Mater.*, 2002, **1**, 123-128.
28. J. L. Allen, T. R. Jow and J. Wolfenstine, *J. Power Sources*, 2011, **196**, 8656-8661.
29. D.-W. Han, Y.-M. Kang, R.-Z. Yin, M.-S. Song and H.-S. Kwon, *Electrochem. Commun.*, 2009, **11**, 137-140.
30. I. Taniguchi, T. N. L. Doan and B. Shao, *Electrochim. Acta*, 2011, **56**, 7680-7685.
31. J. Wolfenstine and J. Allen, *J. Power Sources*, 2004, **136**, 150-153.
32. Z. P. Lin, Y. J. Zhao and Y. M. Zhao, *Chin. Phys. Lett.*, 2009, **26**, 038202.
33. D. Bhuvaneshwari, Gangulibabu, C. H. Doh and N. Kalaiselvi, *Int. J. Electrochem. Sci.*, 2011, **6**, 3714-3728.
34. J. Liu, T. E. Conry, X. Song, L. Yang, M. M. Doeff and T. J. Richardson, *J. Mater. Chem.*, 2011, **21**, 9984-9987.

35. H. J. Zhang, Y. J. Bai, Y. Y. Feng, X. Li and Y. Wang, *Nanoscale*, 2013, **5**, 2243-2248.
36. D. Morgan, A. Van der Ven and G. Ceder, *Electrochem. Solid-State Lett.*, 2004, **7**, A30-A32.
37. G. Chen, X. Song and T. J. Richardson, *Electrochem. Solid-State Lett.*, 2006, **9**, A295-A298.
38. Z. P. Lin, Y. J. Zhao and Y. M. Zhao, *Chin. Phys. Lett.*, 2009, **26**.
39. X. Zhou, F. Wang, Y. Zhu and Z. Liu, *J. Mater. Chem.*, 2011, **21**, 3353-3358.
40. P. Y. Shih, S. W. Yung and T. S. Chin, *J. Non-Cryst. Solids*, 1998, **224**, 143-152.
41. Y. J. Park, Y.-S. Hong, X. Wu, K. S. Ryu and S. H. Chang, *J. Power Sources*, 2004, **129**, 288-295.
42. V. Di Castro and S. Ciampi, *Surf. Sci.*, 1995, **331-333**, Part A, 294-299.
43. N. S. McIntyre and M. G. Cook, *Analytical Chemistry*, 1975, **47**, 2208-2213.
44. N. Bramnik, K. Bramnik, T. Buhrmester, C. Baehtz, H. Ehrenberg and H. Fuess, *J. Solid State Electrochem.*, 2004, **8**, 558-564.



Scheme 1. Illustration of the preparation process of SG@LFCPO.

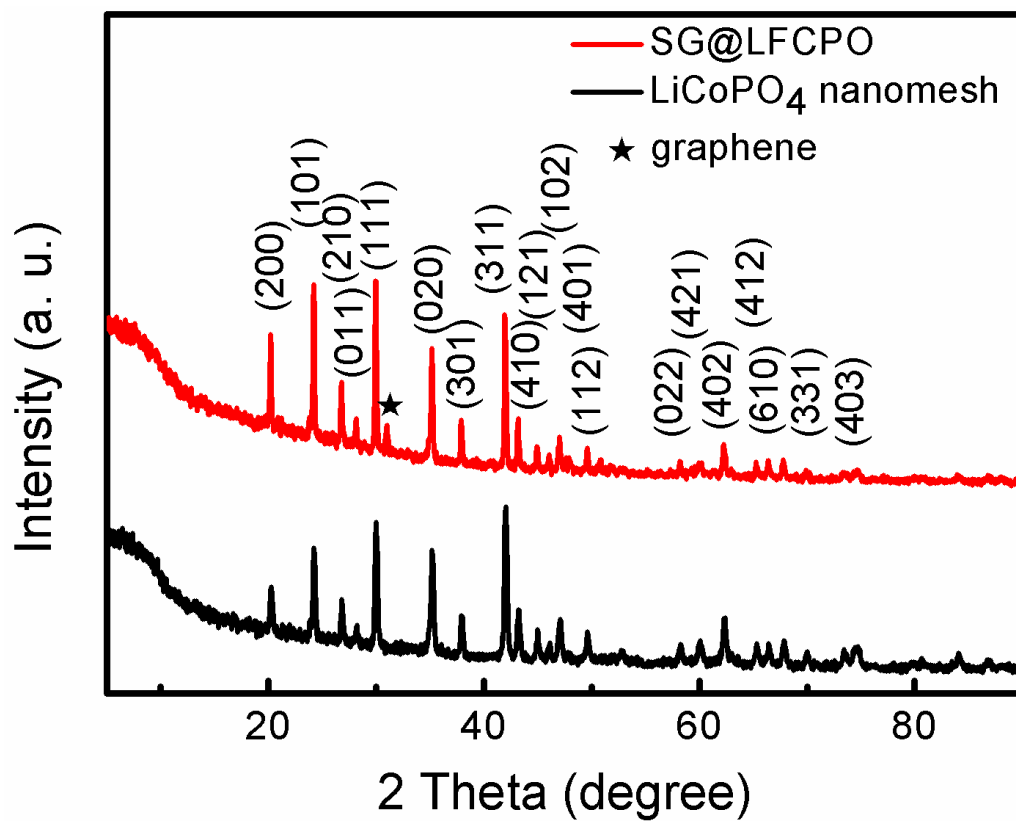


Figure 1. XRD patterns for the SG@LFCPO and LiCoPO₄ nanomesh.

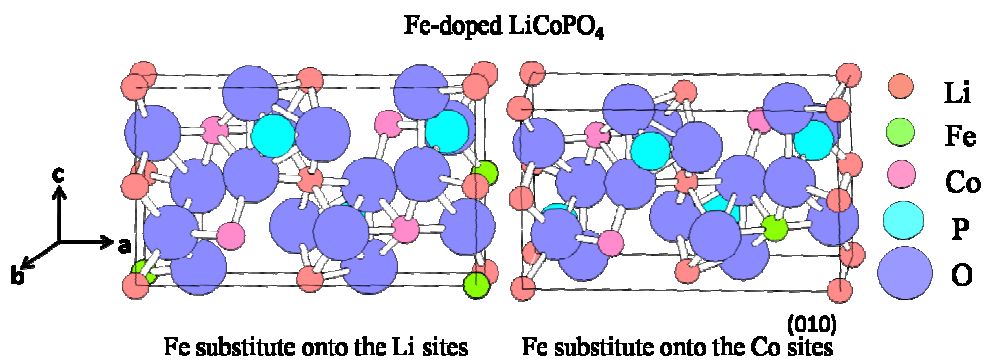


Figure 2. The ball-and-stick model of Fe-doped LiCoPO₄ to illustrate the Li⁺ diffusion pathway along *b* axis direction.

Table 1. Lattice constants for (Li_{0.893}Fe_{0.036})Co(PO₄) and LiCoPO₄, calculated by jade 5.0 software.

	a (Å)	b (Å)	c (Å)
LiCoPO ₄	10.20	5.92	4.700
(Li _{0.893} Fe _{0.036})CoPO ₄	10.21	5.91	4.706

Table 2. Compositions of LiCoPO₄ and SG@LFCPO electrode materials, determined by ICP-AES.

Composites	Targeted Li/Fe/Co ratio	Experimental (ICP-AES) Li/Fe/Co ratio
LiCoPO ₄	1.00:0.00:1.00	0.99:0.001:1.003
SG@LFCPO	0.893:0.036:1.00	0.895:0.032:1.004

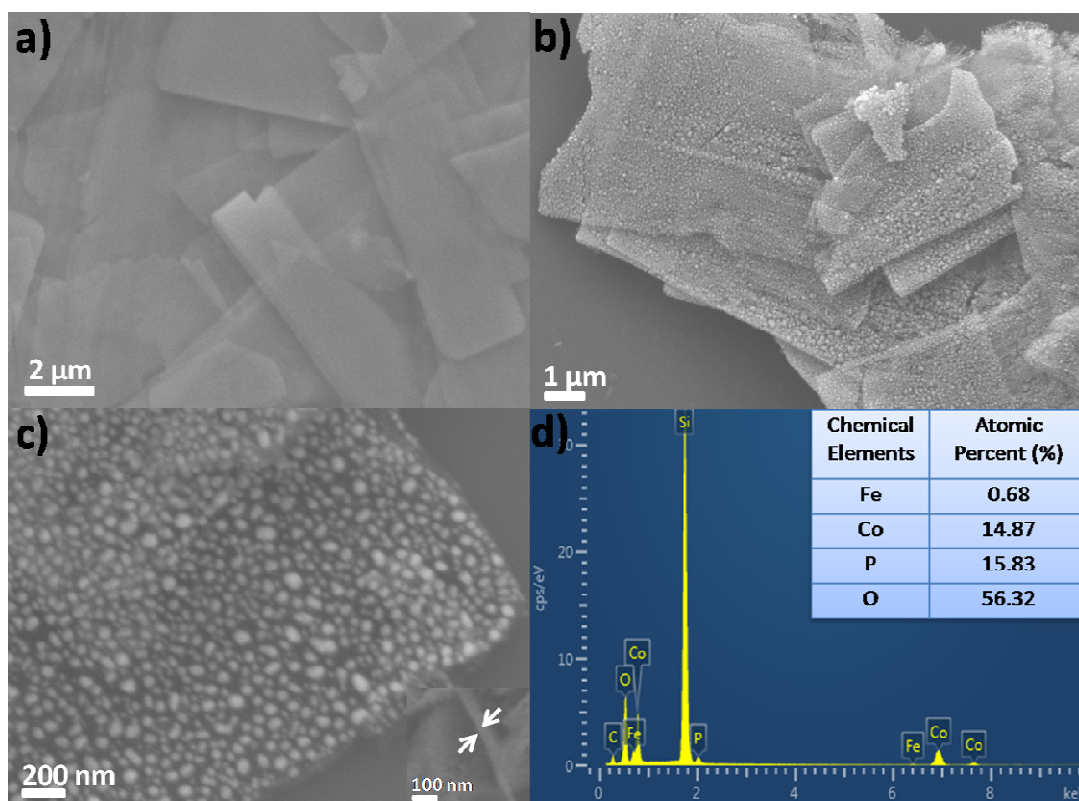


Figure 3. a) SEM image of the $(\text{NH}_4)_2\text{Co}_8(\text{CO}_3)_6(\text{OH})_6 \cdot 4\text{H}_2\text{O}$ sheet-like precursors, b) SEM image of SG@LFCPO, c) High-magnification SEM image of individual SG@LFCPO (the inset image is used to prove the thickness of SG@LFCPO), d) EDS image with the atomic percent data of SG@LFCPO.

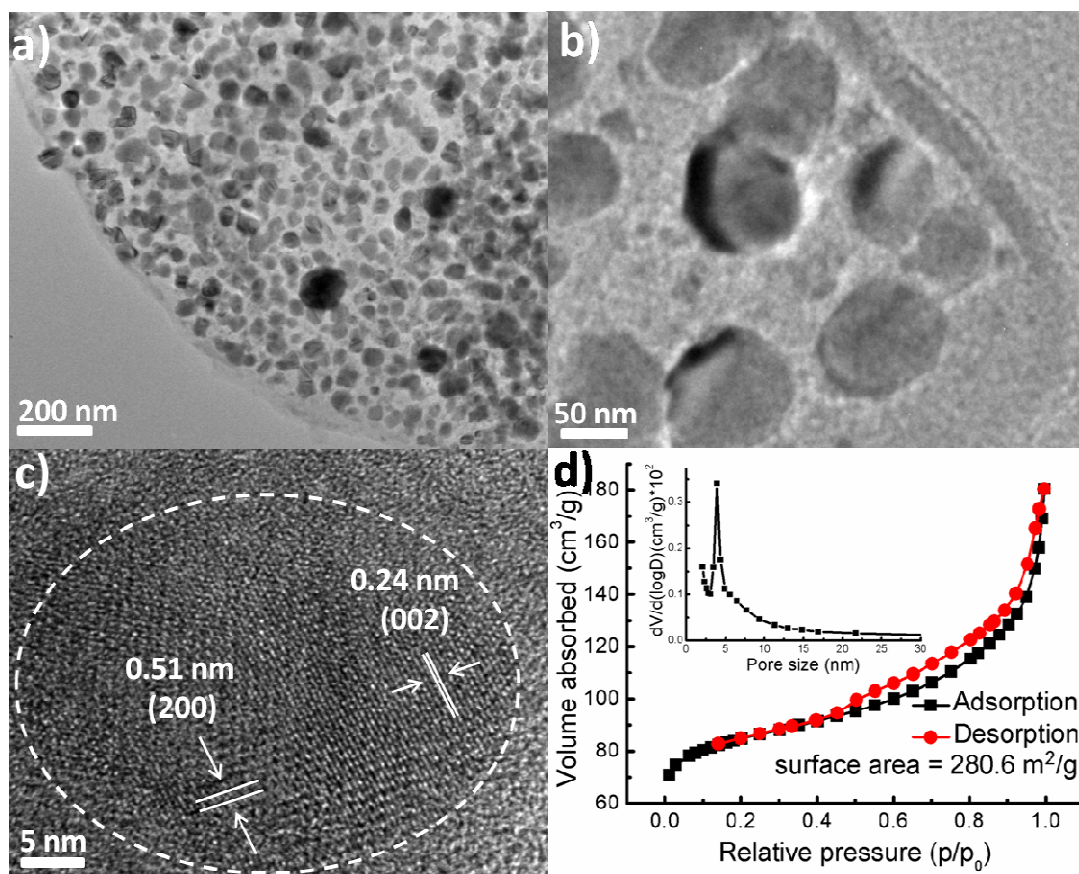


Figure 4. a-b) Stepwise magnified TEM images of SG@LFCPO, c) The locally magnified HRTEM image of SG@LFCPO, d) Nitrogen adsorption-desorption isotherm and the corresponding pore size distribution (inset) of SG@LFCPO.

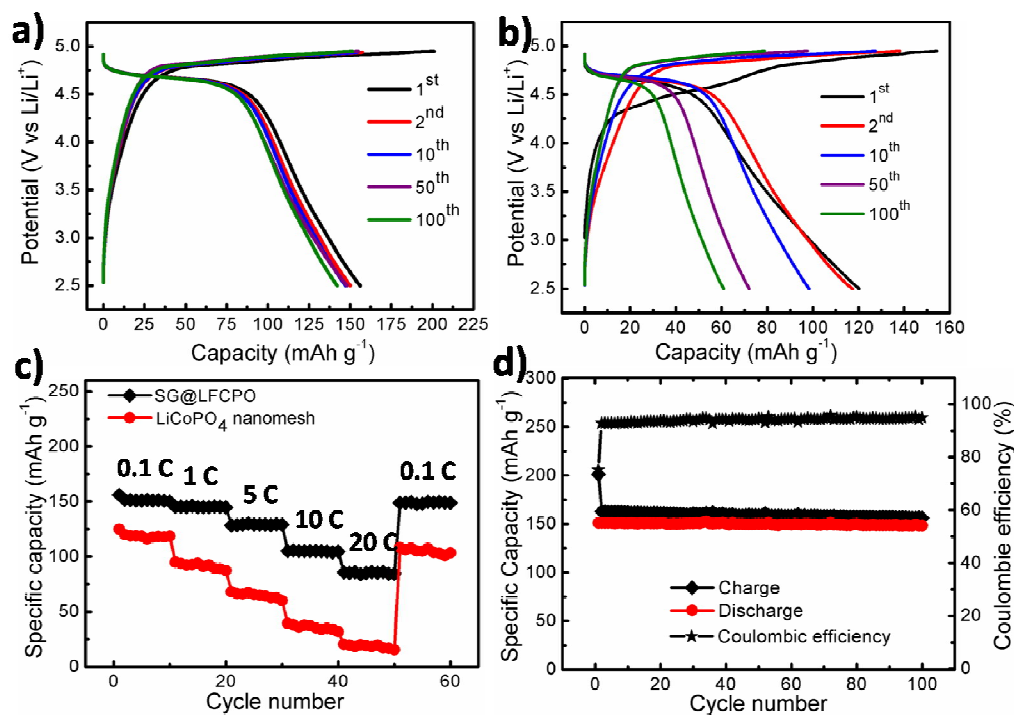
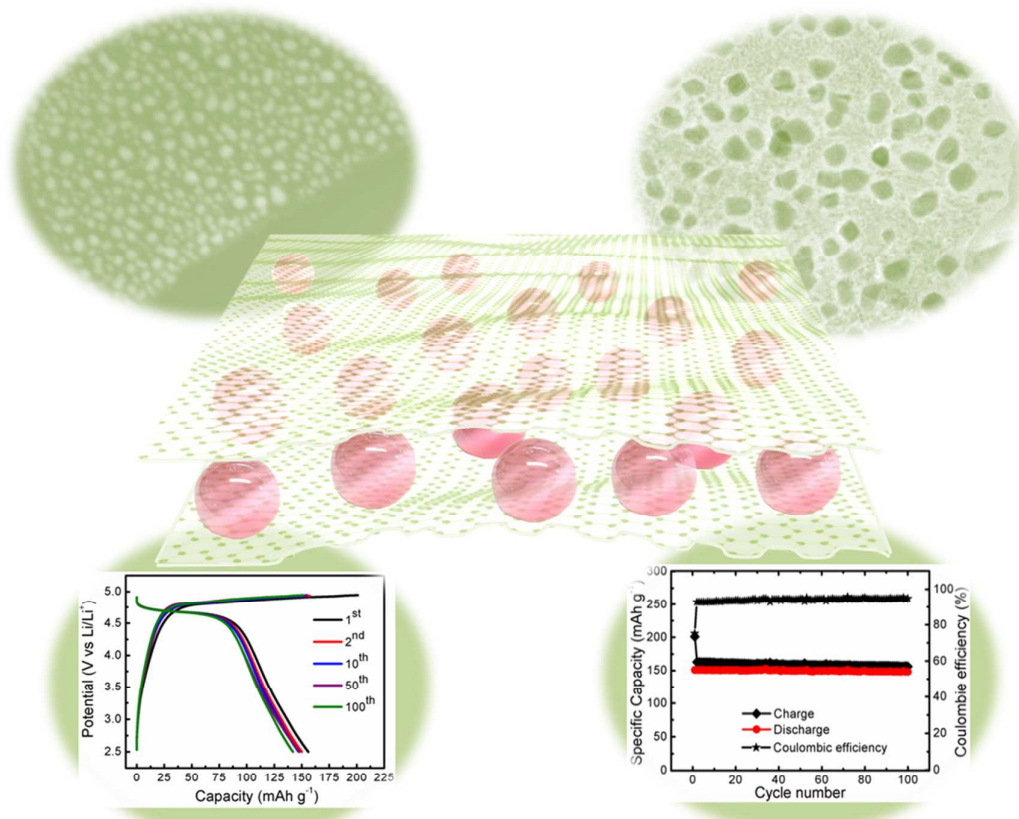


Figure 5. Galvanostatic discharge and charge curves in the voltage range of 2.5-4.95 V vs. Li at 0.1 C of a) SG@LFCPO, b) LiCoPO₄ nanomesh, c) the rate performance at different discharge rates, 0.1, 1, 5, 10 and 20 C, respectively, in the voltage range between 2.5 and 4.95 V of SG@LFCPO and LiCoPO₄ nanomesh, d) the charge-discharge capacities and corresponding coulombic efficiency of SG@LFCPO.

Table of Contents Entry



Herein, the unique two-layered sandwiched graphene@ $(\text{Li}_{0.893}\text{Fe}_{0.036})\text{Co}(\text{PO}_4)$ nanoparticles have been successfully fabricated through the template-sacrificial method. The electrode material takes advantages of the Fe doping, coating graphene and designing the morphology, contributing to outstanding electrochemical performances, such as rate performance (the discharge capacity of 85 mAh g^{-1} at 20 C), cyclability (the coulombic efficiency of around 92.6%), stability (capacity retention of 94.6% after 100 cycles) and fast kinetics. It is believed that our research provides new insights into paving the way for the rational design and realization of graphene-based materials for lithium-ion batteries and related applications.